PAPER • **OPEN ACCESS**

Optical properties of silicon carbide thin films deposited by atomic substitution on porous silicon

To cite this article: Valerii Kidalov *et al* 2025 *Mater. Res. Express* **12** 076402

Materials Research Express

PAPER

Optical properties of silicon carbide thin films deposited by atomic substitution on porous silicon

Valerii Kidalov[1,2], **Lukas Hertling**[3], **Roman Redko**[4], **Volodymyr Dzhagan**[4], **Sergii Mamykin**[4], **Andrey Revenko**[5], **Marc Assmann**[1], **Alena Dyadenchuk**[2,*], **Vitalii Kidalov**[6] and **Dietrich R T Zahn**[3]

[1] Experimentelle Physik 2, Technische Universität Dortmund, Dortmund, Germany
[2] Dmytro Motornyi Tavria State Agrotechnological University, Melitopol, Ukraine
[3] Semiconductor Physics and Research Center for Materials, Architectures and Integration of Nanomembranes (MAIN), Chemnitz University of Technology, Chemnitz, Germany
[4] V Lashkaryov Institute of Semiconductor Physics of the National Academy of Sciences of Ukraine, Kyiv, Ukraine
[5] School of Chemistry, University College Dublin, Belfield, Dublin 4, Ireland
[6] Ruhr-Universität Bochum, Bochum, Germany
[*] Author to whom any correspondence should be addressed.

E-mail: alena.dyadenchuk@tsatu.edu.ua

Keywords: silicon carbide, porous silicon, atomic substitution method, heterostructure, optical properties

OPEN ACCESS

RECEIVED
19 June 2025

REVISED
9 July 2025

ACCEPTED FOR PUBLICATION
15 July 2025

PUBLISHED
24 July 2025

Abstract

Silicon carbide films on porous-Si/Si substrates have attracted considerable attention due to their potential use in modern high-power electronic devices. Here, SiC/porous-Si/Si heterostructures fabricated by an atomic substitution method are investigated. Scanning electron microscopy shows the formation of a continuous about 40 nm thick film of SiC, with a sharp interface to the porous Si sublayer. Energy-dispersive x-ray spectroscopy confirmed that Si, C, and O are the only constituents of the SiC film and the porous-Si underlayer. Raman spectroscopy indicated 3C and 6H polytypes in the SiC film. Spectroscopic ellipsometry in the range of 0.6–5.1 eV was performed in order to determine the refractive index (n), extinction coefficient (k), and bandgap (Eg) of the SiC layer. Macro-FTIR transmission spectra showed the expected absorption features of SiC. IR reflectance maps measured with nano-resolution reveal lateral inhomogeneities of the intensity, which we attribute to the morphology of the porous silicon sublayer. Numerical simulations of the local near-field response were performed for regions, where the SiC layer lay directly on silicon and for regions where it is free-standing over pores. The simulation results are in close agreement with the experimental observations obtained by nanoFTIR and confirm that the porous substrate plays a decisive role in determining the local optical and structural properties of the SiC/porous-Si/Si heterostructures.

1. Introduction

Silicon carbide (SiC) films have attracted considerable attention for decades due to their unique properties, such as high thermal and chemical stability, wide bandgap (2.49–3.26 eV [1]), and high electron mobility (12400 $cm^2/(V{\cdot}s)$ [2]), which make SiC a promising material for appli-cations in high-temperature and high-power electronics as well as for sensors operating in chemi-cally aggressive environments [3]. High-quality SiC films are essential for use in advanced optoe-lectronic devices [4]. To obtain SiC films, various substrates are used such as TiN [5], $SrTiO_3$ [6], and glass [7]. Silicon is a particularly promising substrate for the deposition of SiC films [8].

The integration of the advantageous optical and electrical characteristics of silicon with the superior thermal and electronic properties of silicon carbide (SiC) presents significant opportunities for the development of high-performance electronic and optoelectronic devices [9]. Nevertheless, the realization of high-quality epitaxial growth of SiC films heteroepitaxially deposited on silicon (Si) substrates remains a major challenge. This is primarily due to the substantial lattice mismatch (~20%) between SiC and Si, as well as the pronounced difference in their thermal expansion coefficients [10]. These factors induce high levels of strain and defect

formation such as dislocations and cracks during epitaxial growth and subsequent thermal cycling, ultimately limiting the structural and functional integrity of the resulting heterostructures.

SiC thin films have attracted considerable research interest in the past five years due to their potential applications in high-performance electronics, optoelectronics, and photonic systems. Kavitha *et al* [11] demonstrated that the presence of nitrogen during radio frequency plasma enhanced chemical vapor deposition (RF-PECVD) significantly affects both the structural and photoluminescent properties of SiC films, particularly by tuning the bandgap and enhancing visible emission. Kaloyeros and Arkles [12] provided a comprehensive review of physical vapor deposition (PVD) and alternative non-CVD techniques for SiC film deposition, highlighting how physical growth parameters influence phase formation and morphology. Singh [13] showed that applying external magnetic fields during CVD processes modifies the film growth kinetics and induces magnetic anisotropy, opening new perspectives for magneto-functional device design. Furthermore, Co-doped SiC films were reported to transition from superparamagnetic to ferromagnetic behavior at around 8 at.% Co, suggesting their relevance for spintronic applications [14]. Alzubaidi *et al* [15] applied pulsed laser deposition (PLD) to grow SiC/Si heterostructures, reporting strong photoluminescence in the visible and near-infrared regions suitable for optoelectronic integration. Due to their high thermal conductivity, chemical resistance, and mechanical durability, SiC thin films have become attractive for harsh-environment sensors, including gas and pressure sensors in automotive and aerospace industries [16]. Their wide bandgap also supports UV photodetector applications and integrated photonic circuits [17]. Moreover, rare-earth or defect-engineered SiC thin films have recently emerged as promising platforms for quantum technologies, such as single-photon emitters and spin-based qubits [18]. Their high breakdown voltage and electrical stability make them ideal candidates for substrate in high-power RF with low microwave noise [19].

One promising approach to mitigating these challenges is the atomic substitution method [20]. This method is a heteroepitaxial growth technique, in which carbon monoxide (CO) gas is introduced to react with a silicon (Si) substrate surface at elevated temperatures. This technique involves the controlled replacement of silicon atoms in the substrate surface with carbon atoms, thereby facilitating the formation of a thin interfacial layer gradually changing in composition from Si to SiC. However, a disadvantage of the atomic substitution method is related to the fact that the silicon carbide film is very thin and uneven mechanical stresses arise in it.

We demonstrated [21] that the presence of pores in Si ensures more intense penetration of the CO gas deep into the substrate and, as a consequence, a more 'energetic' rate of the chemical reaction of CO with silicon [22, 23]. In the presence of pores in the substrate, the reaction of con-verting Si into SiC affects a much larger volume of the Si substrate than in the case of the reaction of CO with flat silicon, since the CO gas penetrates into the silicon volume through the pores and the thickness of the silicon carbide film increases [24].

The morphology and internal structure of the SiC films on porous-Si/Si were previously investigated by traditional analytical techniques, such as scanning and transmission electron microscopy (SEM, TEM), atomic force microscopy (AFM), and Raman spectroscopy [25, 26]. Tip-enhanced Raman spectroscopy (TERS) is a powerful technique that allows studying molecular structures and interactions at the nanometer scale, making it an essential tool in nanotechnology, materials science, and biomedical research [27]. Similarly efficient for studying the vibrational spectra of a material with nm-resolution can be another plasmon-enhanced technique based on IR absorption, namely nanoFTIR, which still is an emerging technique [28].

The relevance of this research arises from the growing demand for high-quality SiC films. The atomic substitution method for forming SiC films on porous-Si/Si substrates enables the production of high-quality heterostructures. However, to ensure successful implementation in mass production, it is necessary to carefully optimize the method to meet specific device requirements. Therefore, a key objective is to thoroughly study the properties of the SiC/porous-Si/Si heterostructure obtained, thereby support further technological improvement, and establish optimal conditions for its application in modern electronic devices.

2. Experimental methodology

The process of growing a SiC/porous-Si/Si structure includes the preparation of silicon wafers, the formation of a porous layer by electrochemical etching [29], and the deposition of a SiC film by atomic substitution [21–24, 30]. The method for obtaining SiC/porous-Si/Si heterostructures is described in detail in the works [20–24, 29–31]. The mechanism of silicon carbide film growth on porous Si substrates is described in detail in our previous works [30, 31].

Cross-sectional micrographs of the fabricated structure were obtained using a MIRA3 TESCAN scanning electron microscope equipped with a Bruker XFlash energy-dispersive x-ray spectroscopy (EDX) detector for elemental analysis.

Raman scattering spectra were measured at an excitation wavelength of 514.7 nm with a Horiba LabRam Raman spectrometer (power ~1.8 mW, 100x objective, grating 1/2400 mm, signal accumulation time 6×300 s).

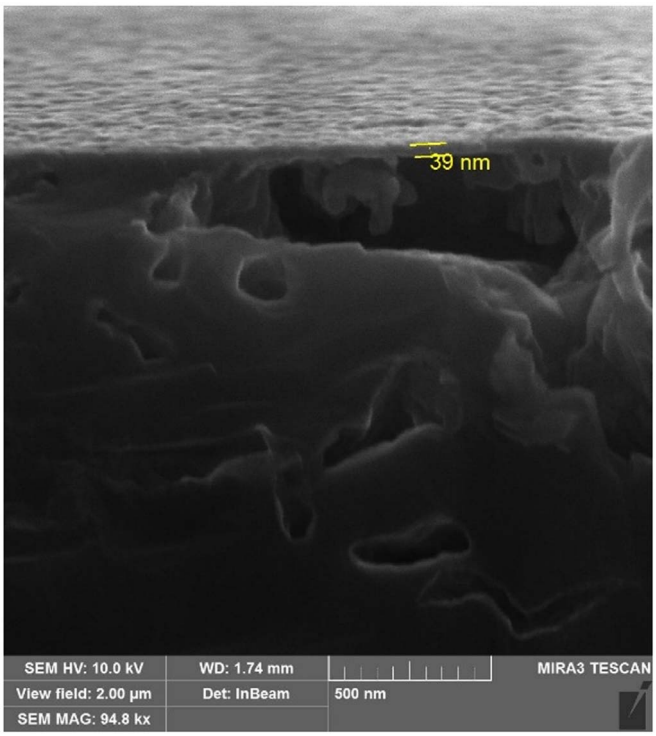

Figure 1. SEM image of the cross-section of the SiC film (thickness marked in yellow) on porous-Si sublayer.

The FTIR measurements were performed in transmission geometry using a Bruker Vertex 80v vacuum FTIR spectrometer. NanoFTIR measurements were taken using an attocube (formerly neaspec) neaSNOM setup. A Toptica Femto Fiberdichromid IR laser was used as a broadband light source. The AFM tip used was a special PtIr-coated tip from attocube. The signal was demodulated at the second harmonic (O_2) in all cases. To study the optical properties of SiC thin films deposited on porous silicon substrates, spectroscopic ellipsometry (SE2000, SemiLab Ltd) in the 0.6–5.1 eV spectral region was used. The analysis aims to determine the thickness, refractive index (n), extinction coefficient (k), and bandgap (E_g) of the SiC layer.

3. Results

The SEM image (figure 1) reveals a very homogeneous and continuous layer of SiC, with a thickness of about 39 nm (marked in the image with yellow bars), formed on top of the porous-Si sublayer. The detailed mechanism of the formation of the flat SiC overlayer on top of the porous Si layer is described in previous works [22–24]. Shortly, the formation of SiC starts on the whole surface of pores, but at some stage the openings of the pores get overgrown and growth inside the pores stops.

Figure 2 shows the result of elemental analysis on the surface of the heterostructure, quantified in table 1. EDX probes a depth down to 2 µm of the sample and thus the obtained composition is an average over the SiC film, the porous Si layer, and Si substrate. In addition to the main substances, a small amount of oxygen is present on the surface. The most likely source of the impurity may be intermediate compounds that arise during the reaction.

For the modelling of the ellipsometry data the thickness of the SiC layer of approximately 40 nm, determined from SEM cross-section images, was used assuming the following structure: Si substrate/porous-Si layer/SiC film/SiC roughness/air. However, modelling of such a 5-layer structure did not give any reasonable agreement with the measured experimental ellipsometry data. This fact, along with the absence of interference fringes in the experimental ellipsometry spectra, indicates that the porous Si sublayer does not contribute as a single layer with effective optical constants. Therefore, we performed modelling assuming separate contribution of the areas with voids and Si walls of the porous-Si layer, in particular; (i) air/SiC film/SiC roughness/air and (ii) continuous (bulk) Si layer/SiC film/SiC roughness/air. In case (i), the modelling did not result in a satisfactory agreement with the experiment, while in case (ii) we obtained very good agreement between theory and experiment, as can be seen in figure 3. So, only those regions of SiC film which are placed on Si (walls) are contributing (dominating) the ellipsometry spectrum in the visible range. The parts of the film which are 'hanging' over the pores are not contributing significantly in the visible range. In particular, an optical model consisting of a 40 nm SiC layer on a

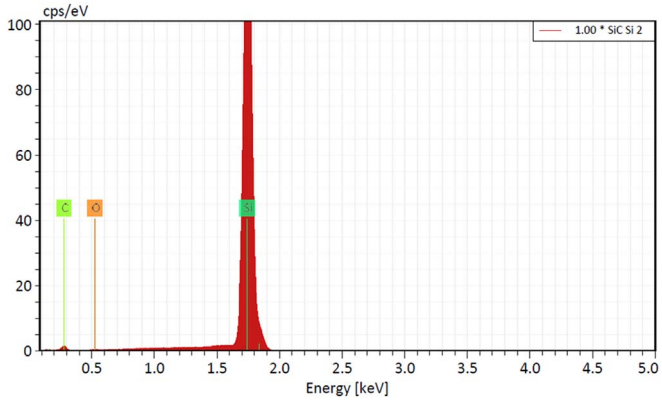

Figure 2. EDX spectrum of the SiC/porous-Si/Si heterostructure surface.

Table 1. Elemental composition of the sample derived from EDX.

Element	Mass Norm., %	Atom, %	Rel. error, % (1 sigma)
C	18.40	34.39	14.45
O	0.61	0.86	26.22
Si	80.99	64.75	4.30
	100	100	

Si substrate with a 5 nm surface roughness layer was used to derive preliminary n and k values (figure 4). An initial rough estimation of the SiC optical constants was performed using a wavelength (WVL) fitting procedure, independently fitting n, k, and the SiC film thickness (40 nm).

To extract the dielectric function of SiC, the Cody-Lorentz model [32] was applied. This model is consistent with Kramers-Kronig relations and usually used to describe the dielectric function of amorphous materials, but also applicable to crystalline materials. It offers improvements over the Tauc-Lorentz model [33] by modifying the joint-density of states (JDOS) and allowing weak exponential absorption below the bandgap.

The Cody-Lorentz model parameters include: A is the oscillator amplitude, E_0 is the oscillator peak position, Γ is the broadening energy, E_g is the bandgap, Ep is the transition energy, E_u is the Urbach tail slope, Et is the demarcation energy, ε_∞ is the high-frequency dielectric constant. The values obtained are shown in table 2.

The analysis in the frame ofThe Cody-Lorentz model yielded a SiC layer thickness of 38.9 ± 1.4 nm and a surface roughness layer thickness of 4.7 ± 3.6 nm. The bandgap (Eg) was determined to be 2.94 ± 0.01 eV. The coefficient of determination (R^2) for the Cody-Lorentz model fit was 0.99806, indicating a high degree of accuracy in the model fit. The determined bandgap value of approximately 2.94 eV suggests that the SiC film may correspond to the 15R-SiC polytype [34], while it is also close to the bandgap of the more common 6H-SiC polytype (~3.0–3.1 eV) [35, 36].

The refractive index (n) and extinction coefficient (k), obtained from the modelling of ellipsometry data, are in good agreement with literature data for bulk SiC and SiC films [37, 38]. For instance, for the visible spectral range, k was found to be 0.047 for the Cody-Lorentz model and 0.074 for the WVL fitting, corresponding to an absorption coefficient $\alpha = 4\pi k/\lambda \approx \sim 10^4$ cm^{-1}, which is in good agreement with reported values [39].

According to the literature [40–43], the characteristic Raman modes of SiC are expected near 200 cm^{-1} and below 1000 cm^{-1}, while their number and frequency position depends on the particular polytype [40–45]. In the low-frequency part of the spectrum of the SiC/porous-Si/Si heterostructure studied in this work, a broad band with maxima at about 125 and 154 cm^{-1} is observed (figure 4(a)). The former can be assigned to the folded transversal acoustic (FTA) mode of the 21-R polytype, and the latter to the analogous mode of the 6H-SiC polytype, since the other polytypes do not have modes in this range [34]. Based on this assignment, the mode at 794 cm^{-1} can be associated with the planar optical folded transversal optical (FTO) mode of the 6H-SiC polytype [40]. However, the good coincidence of the peak at 794 cm^{-1} with the TO phonon frequency for the 3C-SiC polytype [41] (and the TA phonons at 125 and 154 cm^{-1} for the 6H-SiC polytype) may indicate the presence of a certain combination of the two polytypes in the thin film. The co-existence of several polytypes of thin SiC films grown on porous Si by the same technique was proven by XRD earlier [22].

The high-frequency Raman spectrum of the SiC/porous-Si/Si heterostructure is shown in figure 4(b). The strong and broad (trapezoidal) band at 950–1000 cm^{-1} is mainly due to second-order scattering from the silicon

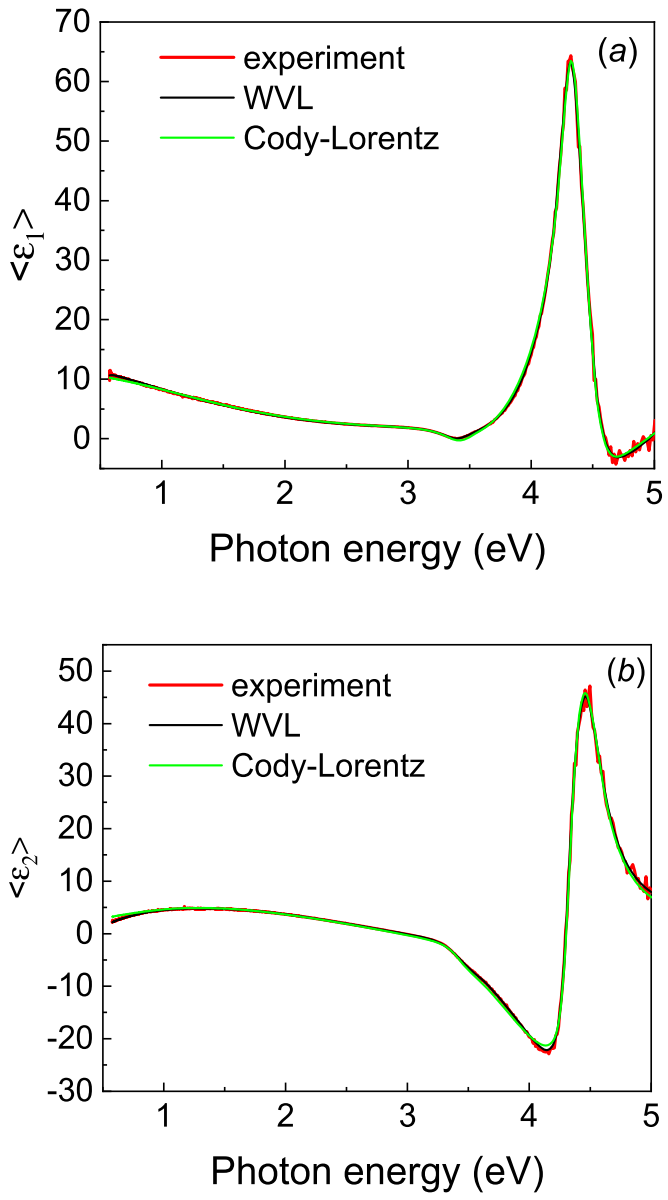

Figure 3. Spectral dependences of the real and imaginary part of the effective dielectric function $\langle\varepsilon_1\rangle$ (a) and $\langle\varepsilon_2\rangle$ (b) of the SiC film on Si, and its modeling using WVL fitting and the Cody-Lorenz model.

substrate. However, the sharp peak at 942 cm^{-1} on top of it can be associated with the LO phonon of 3C-SiC. Usually, the LO phonon for 3C-SiC is observed at 970–975 cm^{-1}, so the lower frequency value may be related with the effect of residual strain in the SiC film. In addition, we most likely have a film of the 3C-SiC polytype with fragments of the 6H-SiC polytype and possibly also 21-R, so the peak at 942 cm^{-1} may be related with these phases. Broad bands near 825 cm^{-1} and 980 cm^{-1} can be associated with amorphous SiC phases [42, 43], since bands in these ranges and with similar shape were observed during the formation of various combinations of Si-H, Si-CH_3, Si-C bonds using silane gas (SiH_4) [42], which was also used in our fabrication process.

Prior to investigation of near-field nanoFTIR, a macroscopic Fourier transform infrared (FTIR) spectrum measured in transmission was acquired (figure 5). The expected absorption band for SiC fromabout 780 cm^{-1} to about 900 cm^{-1} is observed (figure 6). The weak feature at 700 cm^{-1} may be related with one of the SiC polytypes, because it is not characteristic for Si-Si or Si-O bonds. Distinguishing different polytypes is not possible due to large bandwidth in the IR spectra (as compared to the Raman ones). The extremely low transmission in the high-frequency region (>1000 cm^{-1}) of the spectrum is unusual. Most likely, the intense absorption of the signal in this region of the spectrum occurs predominantly due to losses in the porous silicon sublayer hindering determination of the SiC layer contribution in this spectral range. The additional features near 600 cm^{-1} and 950 cm^{-1} were previously identified as Si-H wagging modes [46, 47] and Si–O–Si stretching modes [48], respectively. Other work assigned the feature near 950 cm^{-1} to C-Hn wagging modes while also considering the one at 1100 cm^{-1} to be due to the asymmetric Si–O–Si stretching mode [41, 49, 50].

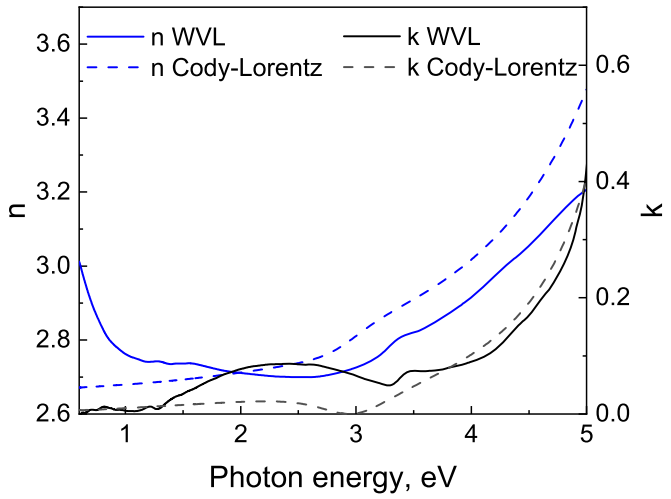

Figure 4. Spectral dependences of the refractive index of the SiC film obtained using WVL fitting and the Cody-Lorenz model.

Table 2. Parameters of the Cody-Lorentz model for describing the dielectric function of a SiC film.

d(nm)	38.9 ± 1.4
A (eV)	13.68 ± 2.2
E_0 (eV)	5.89 ± 0.08
Γ (eV)	0.805 ± 0.02
E_g (eV)	2.94 ± 0.01
E_p (eV)	0.435 ± 0.04
E_u (eV)	0.42 ± 0.4
E_t (eV)	1.00 ± 2.0
ε_∞	4.93 ± 0.3
R^2	0.99806

To investigate the possible influence of the film morphology on the absorption in the range of 800–1500 cm^{-1}, near-field nanoFTIR measurements were performed comprising measurements of the near-field IR amplitude signal (figure 7, right) and the simultaneously recorded AFM film topography (figure 7, left). The near-field amplitude is often interpreted as a measure of the reflection [44]. The dark areas in figure 7 (right) thus correspond to regions of stronger absorption. The very strong contrast between different areas in the IR amplitude map does not correlate with the rather uniform morphology of the film obtained from AFM. This indicates a minimal contribution of the morphology (or film thickness) to the observed variation of the IR amplitude signal. It is thus suggested that the intensity inhomogeneities in the IR reflectance map are associated with the porous structure of the substrate under the film, in particular, the areas of low reflection (dark) are located above the pores in the silicon substrate.

To clarify the differences between the dark and light areas in figure 7(right), nanoFTIR spectra were measured. The results are presented in figure 8. The measured signal is proportional to the scattering coefficient of the near-field signal and is generally quite complex. Typically, when interpreting the signal from organic materials, it is assumed that the phase (shown on the *y*-axis in figure 8) is proportional to absorption [51, 52]. For strong oscillators such as SiC, the phase and amplitude can shift to the LO mode position.

For bulk 4H-SiC, the phase signal exhibits a peak ~950 cm^{-1} [44] (figure 9). For the studied SiC thin films, the spectrum is more complex and differs in the dark and bright areas. In the bright areas it shows and sharper peak slightly above 950 cm^{-1} and a broader one below 950 cm^{-1}. In the dark areas, an additional broad feature between 800 and 900 cm^{-1} is observed (figure 8). Explaining this requires modeling of the near-field response. Generally, the modelling of multilayers follows a similar path, irrespective of using a Point-Dipole-Model [52], a Finite-Dipole-Model [53], or a more advanced approach [54, 55]. In all cases, the sample is described using momentum-dependent Fresnel reflection coefficients of multilayers instead of the quasistatic reflection coefficients used for bulk samples while the tip is described as a dipole of various shapes. The tip-sample system modelling the near-field response is most sensitive to a certain momentum range, which is often expressed by a

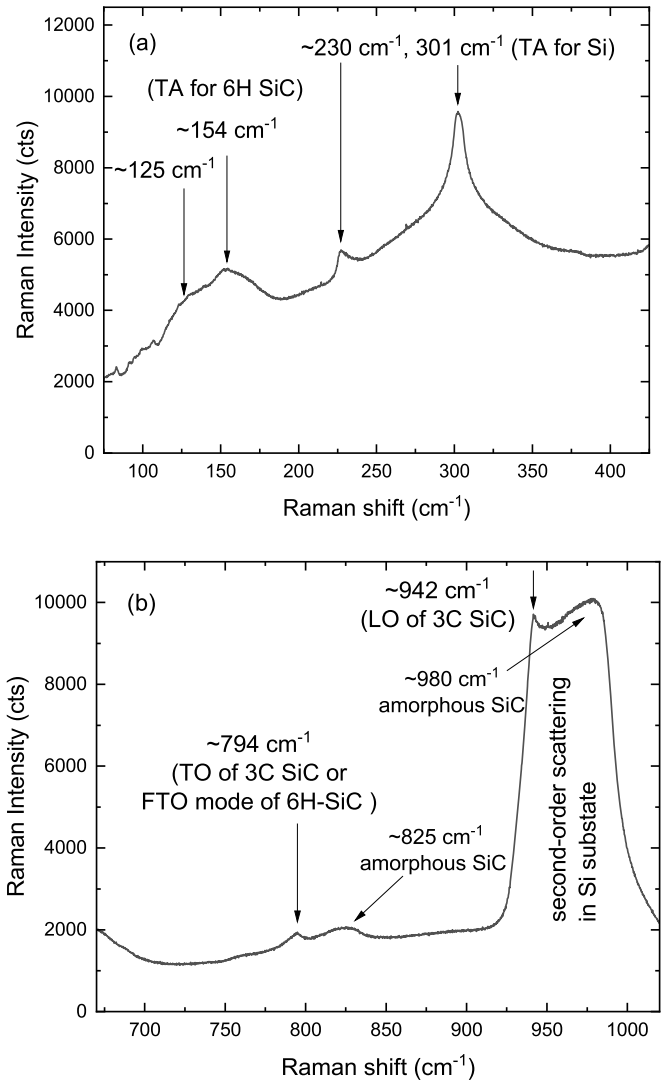

Figure 5. Raman spectra of the SiC/porous-Si/Si heterostructure in the range 100–400 cm^{-1} (a) and 700–1000 cm^{-1} (b). The broad feature between 925 and 1000 cm^{-1} is mainly due to second-order scattering in Si substrate, but the possible additional contribution of SiC film in this spectral range is also indicated.

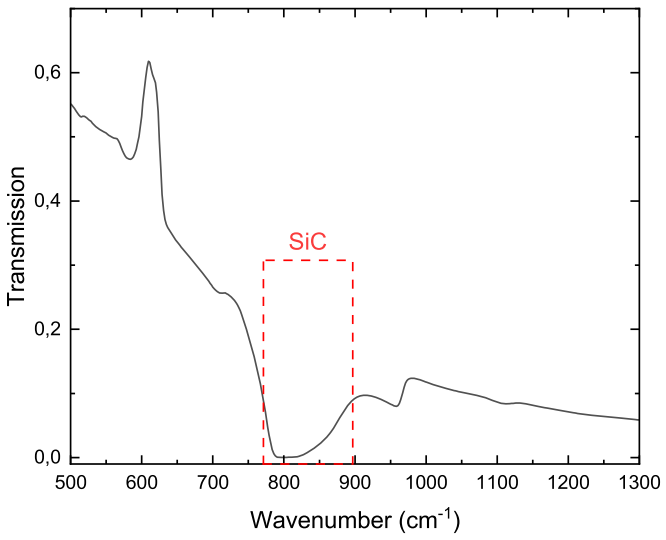

Figure 6. Macro FTIR spectrum of the SiC/porous-Si/Si heterostructure.

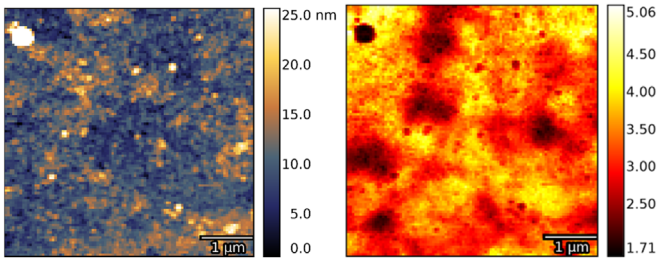

Figure 7. AFM topography (left) and near-field IR amplitude (right) maps of the SiC/porous-Si/Si heterostructure. The illumination range used for the near-field map is approx. 800—1600 cm^{-1}.

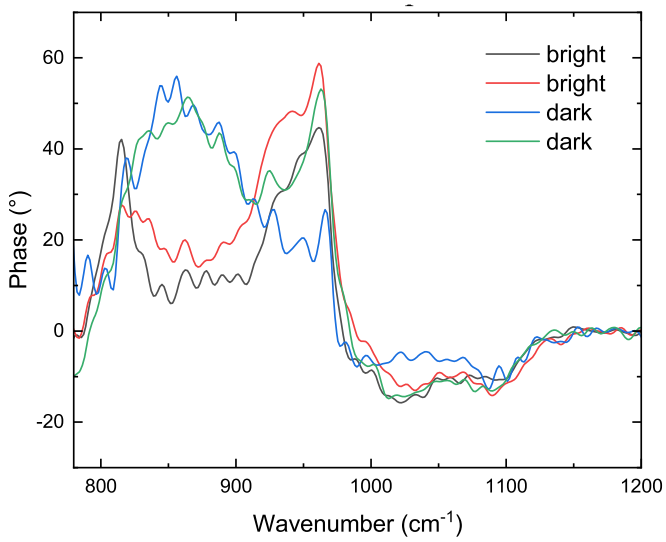

Figure 8. Near-field IR phase spectra in dark and bright areas of the sample.

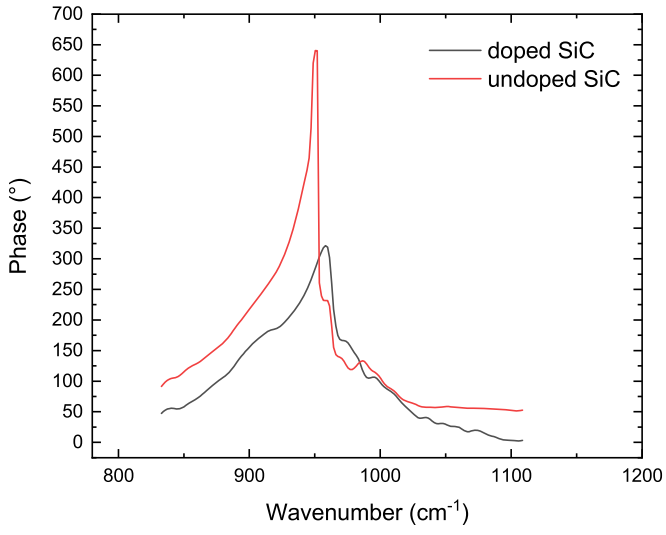

Figure 9. Near-field IR phase spectra of n-doped (approx. $5{\cdot}10^{18}$ cm^{-3}) and nominally undoped bulk SiC.

coupling weight function. This function with a shape similar to a Gaussian function depends on the system geometry, especially the tip radius. In the above-mentioned references of the different models [53–55] the calculated coupling weight function shows that the momentum probed by the tip is in the range of 10^4–10^5

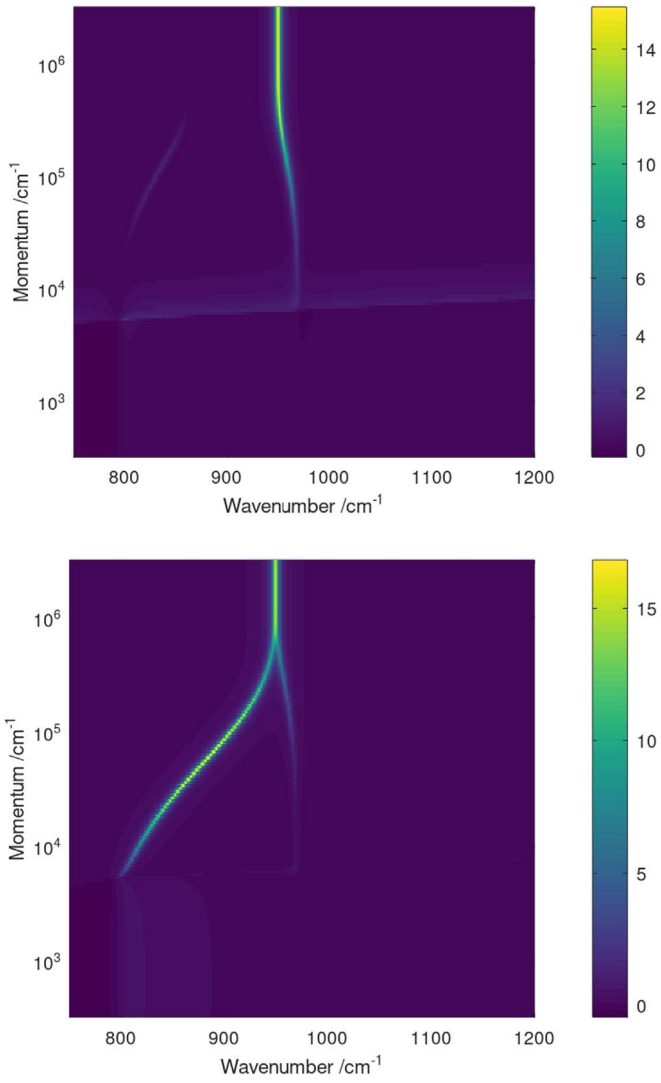

Figure 10. The imaginary part of the Fresnel reflection coefficient for the air-SiC-Si (up) and air-SiC-air (down) systems.

cm^{-1}. We can then estimate the expected near-field response by inspecting the modeled Fresnel reflection coefficients of the system investigated.

For this, we separated the SiC/porous-Si/Si heterostructure into two systems. One layer stack of air-SiC-Si, representing the parts of the sample, where the SiC is directly on top of the silicon substrate, and one layer stack of air-SiC-air representing those parts of the sample, where the SiC layer is above a pore in silicon. We used the usual dielectric constant of 11.7 for silicon and took the dielectric function of SiC from literature [56]. Figure 10 shows the imaginary part of the Fresnel reflection coefficients for those two systems. Within the probed momentum range of 10^4–10^5 cm^{-1}, the air-SiC-Si system shows a weak feature just above 800 cm^{-1} and a stronger one near 950 cm^{-1}. Both features show little dispersion. This corresponds well to the spectra measured on the brighter spots showing two relatively sharp features at those wavenumbers. In contrast, the air-SiC-air system, while possessing an almost identical feature near 950 cm^{-1}, shows a strong feature at lower wavenumbers. This feature has a strong dispersion ranging from 800 to 900 cm^{-1} within the range of the probed momentum. This again corresponds well to the spectra measured on the dark parts, which show a similarly sharp feature near 950 cm^{-1} while also having a far broader feature right within the wavenumber range estimated here. It is therefore reasonable to assume that the bright and dark spots in figure 7 correspond to regions of SiC above silicon and above pores, respectively.

4. Conclusions

The SiC film obtained on porous-Si/Si substrate by atomic substitution method exhibit very homogeneous thickness (about 40 nm), small roughness of the surface (about 5 nm), and a sharp interface with the porous-Si sublayer. Raman scattering spectra revealed vibrational modes corresponding to 3C-SiC, 6H-SiC, and possibly

21-R polytypes. Broad bands were also detected that may be associated with amorphous SiC phases. Spectral ellipsometry, combined with appropriate optical modeling by a Cody-Lorentz model offers a suitable approach to characterize the optical functions of the studied SiC film, yielding accurate values for thickness, refractive index, extinction coefficient, and bandgap. The determined bandgap (2.94 eV) suggests the possible presence of the 6H-SiC polytype. The derived optical constants of the SiC layer are in good agreement with other works [37, 38]. According to ellipsometry measurements, the optical properties in the UV-NIR range of the structure under investigation caused by the areas where the film lies on solid silicon, while in the far-IR range, the areas where the film is formed over cavities play a significant role. Experimental FTIR and nanoFTIR results, corroborated by numerical modelling, indicate a significant contribution of the porous substrate on the IR reflection of the SiC film. The SiC films investigated in the present paper, which exhibit increased absorbance in the 800–1000 cm^{-1} spectral range, may be applied as an effective buffer layer for multilayer structures in sensor applications.

Acknowledgments

The study was partially supported by the National Academy of Sciences of Ukraine (Projects #0125U000799, 0125U000995), the German Research Foundation under the Walter Benjamin Programme, referenced as KI 2865/1-1, and Science Foundation Ireland under the Supplemental Grant for Displaced Researchers scheme (SFI 20/FFP-P/8728 (S)).

Data availability statement

The data cannot be made publicly available upon publication because they are not available in a format that is sufficiently accessible or reusable by other researchers. The data that support the findings of this study are available upon reasonable request from the authors.

Author contributions

Valerii Kidalov 0000-0002-5128-1880
Investigation (equal)

References

[1] Hoat D M, Naseri M, Hieu N N, Ponce-Pérez R, Rivas-Silva J F and Cocoletzi G H 2020 *Superlattices Microstruct.* **137** 106320
[2] Pernot J, Contreras S, Camassel J, Robert J L, Zawadzki W, Neyret E and Di Cioccio L 2000 *Appl. Phys. Lett.* **77** 4359
[3] Zhang Q, Liu Y, Li H, Wang J, Wang Y, Cheng F and Zhang P 2024 *Sensors* **24** 7731
[4] La Via F, Alquier D, Giannazzo F, Kimoto T, Neudeck P, Ou H and Tudisco S 2023 *Micromachines* **14** 1200
[5] Pogrebnjak A D, Ivashchenko V I, Skrynskyy P L, Bondar O V, Konarski P, Załęski K and Coy E 2018 *Composites* B **142** 85
[6] Oujja M, Tabakkouht K, Sanz M, Rebollar E, Sánchez-Arenillas M, Marco J F and de Nalda R 2022 *Appl. Phys.* A **128** 375
[7] Xu J, Wang C, Li D, Cheng J, Wang Y, Hang C and Tian Y 2019 *Ceram. Int.* **45** 4094
[8] Foisal A R M, Nguyen T, Dinh T, Nguyen T K, Tanner P, Streed E W and Dao D V 2019 *ACS Appl. Mater. Interfaces* **11** 40980
[9] Song S, Gao Z, Lu B, Bao C, Zheng B and Wang L 2020 *Ceram. Int.* **46** 568
[10] Reeber R R and Wang K 2000 *MRS Online Proceedings Library (OPL)* **622** 35
[11] Kavitha V S, Kumar R and Narayan J 2025 *Silicon* **17**
[12] Kaloyeros A E and Barry A 2024 *ECS J. Solid State Sci. Technol.* **13** 043001
[13] Singh B 2025 *J. Mater. Chem. A* **13**
[14] Kumar M, Singh A K, Kumar A, Kumar R, Gautam Y K, Dash S K and Chandra R 2025 *Next Nanotechnology* **7** 100110
[15] Alzubaidi R, Fakhri M A and Pohl L 2025 *Thermo* **5** 13
[16] Zhang Q, Liu Y, Li H, Wang J, Wang Y, Cheng F, Han H and Zhang P 2024 *Sensors* **24** 7731
[17] Zhang W, Chen Y X, Yang J Y, Feng S Y, Li B, Lu W E, Liu F Y and Wan J 2025 *IEEE Trans. Electron Devices* **72** 2411–6
[18] Zhou Y *et al* 2025 *Appl. Phys. Rev.* **12** 031301
[19] Zhou M *et al* 2025 *IEEE Trans. Electron Devices* **72** 2874–8
[20] Kidalov V V, Kladko V P, Dyadenchuk A F, Gudymenko O I, Baturin V A and Karpenko A Y 2022 *Nanosistemi, Nanomateriali, Nanotehnologii* **20** 647–55
[21] Kidalov V V, Kukushkin S A, Osipov A V, Redkov A V, Grashchenko A S, Soshnikov I P and Dyadenchuk A F 2018 *ECS J. Solid State Sci. Technol.* **7** P158
[22] Kidalov V V, Kukushkin S A, Osipov A V, Redkov A V, Grashchenko A S, Soshnikov I P and Dyadenchuk A F 2018 *Journal of Nano-and Electronic Physics* **10** 03026
[23] Kidalov V V, Revenko A S, Duleba D, Redko R A, Assmann M, Gudimenko A I and Johnson R P 2024 *ECS J. Solid State Sci. Technol.* **13** 114003
[24] Kukushkin S A, Sharofidinov S S, Osipov A V, Redkov A V, Kidalov V V, Grashchenko A S, Soshnikov I P and Dydenchuk A F 2018 *ECS J. Solid State Sci. Technol.* **7** P480

[25] Torchynska T V, Morales Rodríguez M, Vivas Hernandez A, Polupan G, Jiménez Sandoval S, Ostapenko S and Mynbaeva M 2005 *Physica Status Solidi* (C) **2** 2962
[26] Yukhymchuk V O, Kiselov V S, Valakh M Y, Tryus M P, Skoryk M A, Rozhin A G and Belyaev A E 2016 *J. Phys. Chem. Solids* **91** 145
[27] Verma P 2017 *Chem. Rev.* **117** 6447
[28] Milekhin A G, Kuznetsov S A, Sveshnikova L L, Duda T A, Milekhin I A, Rodyakina E E and Zahn D R T 2017 *The Journal of Physical Chemistry C* **121** 5779
[29] Kidalov V V, Dyadenchuk A F, Baturin V A, Karpenko O Y, Kolomys O F, Ponomarenko V V and Okhrimenko O B 2023 *Semiconductor Physics, Quantum Electronics & Optoelectronics* **26** 140
[30] Kidalov V, Dyadenchuk A, Abbasova C, Baturin V, Karpenko O, Gudimenko O and Kidalov V 2022 Synthesis and characterization of SiC-based thin film heterostructures *2022 IEEE 12th Int. Conf. Nanomaterials: Applications & Properties (NAP)* (IEEE) 01–04
[31] Kidalov V V, Dyadenchuk A F, Zhuk A G, Gudimenko O Y and Simchenko S V 2024 *Himia, Fizika ta Tehnologia Poverhni* **15** 221
[32] Ferlauto A S, Ferreira G M, Pearce J M, Wronski C R, Collins R W, Deng X and Ganguly G 2002 *J. Appl. Phys.* **92** 2424
[33] Jellison G E Jr and Modine F A 1996 Erratum:Parameterization of the optical functions of amorphous materials in the interband region [1996 *Appl. Phys. Lett.* **69** 371] *Appl. Phys. Lett.* **69** 2137
[34] Rohmfeld S, Hundhausen M, Ley L, Zorman C A and Mehregany M 2002 *J. Appl. Phys.* **91** 1113
[35] Choyke W J, Hamilton D R and Patrick L 1964 *Phys. Rev.* **133** A1163
[36] Kimoto T and Cooper J A 2014 *Fundamentals of Silicon Carbide Technology: Growth, Characterization, Devices and Applications* (Wiley) (https://doi.org/10.1002/9781118313534)
[37] Sridhara S G, Eperjesi T J, Devaty R P and Choyke W J 1999 *Materials Science and Engineering: B* **61** 229
[38] Larruquert J I, Pérez-Marín A P, García-Cortés S, Rodríguez-de Marcos L, Aznárez J A and Méndez J A 2011 *Journal of the Optical Society of America A* **28** 2340–5
[39] Solangi A and Chaudhry M I 1992 *J. Mater. Res.* **7** 539
[40] Espinosa-Torres N D, la Luz D H D, Flores-Gracia J F J, Luna-López J A, Martínez-Juárez J and Vázquez-Valerdi D E 2014 *Nanoscale Res. Lett.* **9** 1
[41] Bauer M, Gigler A M, Huber A J, Hillenbrand R and Stark R W 2009 *J. Raman Spectrosc.* **40** 1867
[42] Nakashima S and Harima H 1997 *Physica Status Solidi (a)* **162** 39
[43] Inoue Y, Nakashima S, Mitsuishi A, Tabata S and Tsuboi S 1983 *Solid State Commun.* **48** 1071
[44] El Khalfi A-I, Ech-Chamikh E M, Ijdiyaou Y, Azizan M, Essafti A, Nkhaili L and Outzourhit A 2014 *Spectrosc. Lett.* **47** 392
[45] Costantini J-M, Miro S and Pluchery O 2017 *J. Phys. D* **50** 095301
[46] Ivashchenko L, Vasin A, Ivashchenko V, Ushakov M and Rusavsky A 2005 *MRS Online Proceedings Library* **910** 1203
[47] Shariatmadar Tehrani F *et al* 2013 *J. Mater Sci: Mater Electron* **24** 1361
[48] Luo G, Zhang Z, Hu J, Zhang J, Sun Y, Shen Q and Zhang L 2020 *Materials* **13** 1496
[49] Kaneko T, Nemoto D, Horiguchi A and Miyakawa N 2005 *J. Cryst. Growth* **275** e1097
[50] Merazga S, Keffous A, Brighet A and Kechouane M 2017 *Nano World Journal* **3** 54
[51] Mester L, Govyadinov A, Chen S, Goikoetxea M and Hillenbrand R 2020 *Nat. Commun.* **11** 3359
[52] Aizpurua J, Taubner T, Garcia de Abajo F, Brehm M and Hillenbrand R 2008 *Opt. Express* **16** 1529
[53] Hauer B, Engelhardt A and Taubner T 2012 *Opt. Express* **20** 13173
[54] Jiang B, Zhang L, Castro Neto A, Basov D and Fogler M 2016 *J. Appl. Phys.* **119** 054305
[55] McLeod A, Kelly P, Goldflam M, Gainsforth Z, Westphal A, Dominguez G, Thiemens M, Fogler M and Basov D 2014 *Phys. Rev. B* **90** 085136
[56] Dong J, Zhao J and Liu L 2017 *J. Quant. Spectrosc. Radiat. Transf.* **197** 114